Relationship Between Fine-Particle Pollution and the Urban Heat Island in Beijing, China: Observational Evidence

Zuofang Zheng, Guoyu Ren, Hong Wang, Junxia Dou, Zhiqiu Gao, Chunfeng Duan, Yubin Li, Jean Paul Ngarukiyimana, Chun Zhao, et al.

Boundary-Layer Meteorology
An International Journal of Physical, Chemical and Biological Processes in the Atmospheric Boundary Layer

ISSN 0006-8314

Boundary-Layer Meteorol
DOI 10.1007/s10546-018-0362-6

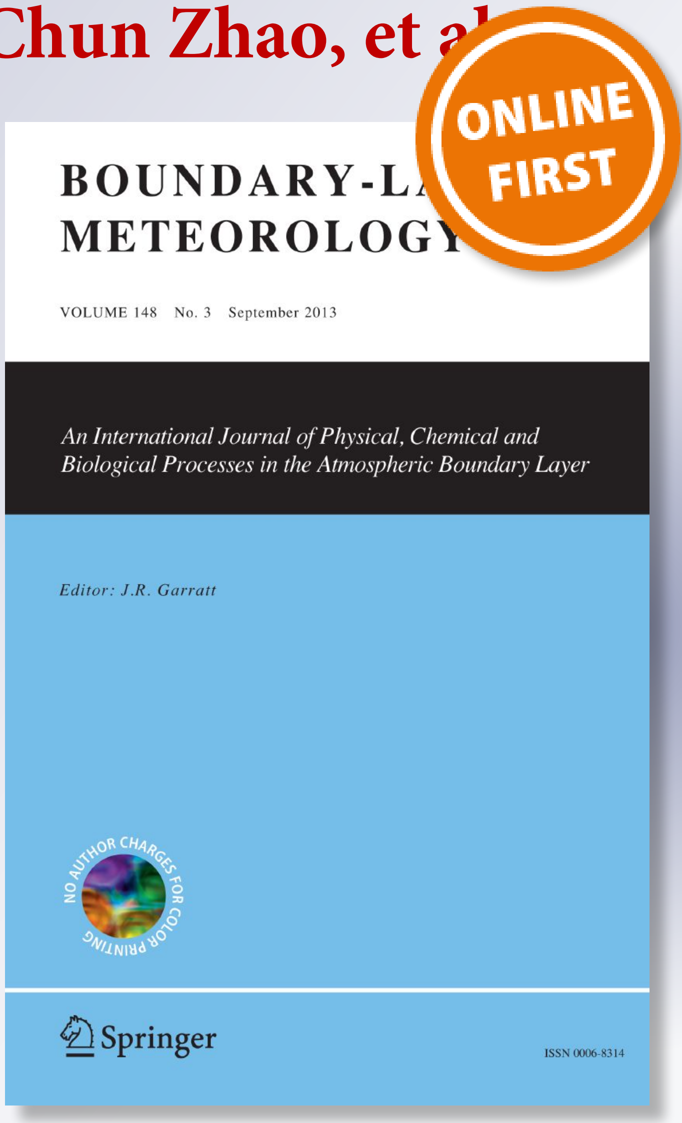

Springer

Boundary-Layer Meteorol
https://doi.org/10.1007/s10546-018-0362-6

RESEARCH ARTICLE

Relationship Between Fine-Particle Pollution and the Urban Heat Island in Beijing, China: Observational Evidence

Zuofang Zheng[1] · **Guoyu Ren**[2,3] · **Hong Wang**[4] · **Junxia Dou**[1] · **Zhiqiu Gao**[4] · **Chunfeng Duan**[5] · **Yubin Li**[4] · **Jean Paul Ngarukiyimana**[6] · **Chun Zhao**[6] · **Chang Cao**[4] · **Mei Jiang**[4] · **Yuanjian Yang**[4]

Received: 25 July 2017 / Accepted: 03 May 2018

Abstract Urbanization has led to a significant urban heat island (UHI) effect in Beijing in recent years. At the same time, air pollution caused by a large number of fine particles significantly influences the atmospheric environment, urban climate, and human health. The distribution of fine particulate matter ($PM_{2.5}$) concentration and its relationship with the UHI effect in the Beijing area are analyzed based on station-observed hourly data from 2012 to 2016. We conclude that, (1) in the last five years, the surface concentrations of $PM_{2.5}$ averaged for urban and rural sites in and around Beijing are 63.2 and 40.7 $\mu g\ m^{-3}$, respectively, with significant differences between urban and rural sites ($\Delta PM_{2.5}$) at the seasonal, monthly and daily scales observed; (2) there is a large correlation between $\Delta PM_{2.5}$ and the UHI intensity defined as the differences in the mean (ΔT_{ave}), minimum (ΔT_{min}), and maximum (ΔT_{max}) temperatures between urban and rural sites. The correlation between $\Delta PM_{2.5}$ and ΔT_{min} (ΔT_{max}) is the highest (lowest); (3) a Granger causality analysis further shows that $\Delta PM_{2.5}$ and ΔT_{min} are most correlated for a lag of 1–2 days, while the correlation between $\Delta PM_{2.5}$ and ΔT_{ave} is lower; there is no causal relationship between $\Delta PM_{2.5}$ and ΔT_{max}; (4) a case analysis shows that downwards shortwave radiation at the surface decreases with an increase in $PM_{2.5}$ concentration, leading to a weaker UHI intensity during the daytime. During the night, the outgoing longwave radiation from the surface decreases due to the presence of

✉ Yuanjian Yang
yyj1985@nuist.edu.cn

[1] Institute of Urban Meteorology, China Meteorological Administration, Beijing 100089, China

[2] Department of Atmospheric Science, School of Environmental Studies, China University of Geosciences, Wuhan 430074, China

[3] Laboratory for Climate Studies, National Climate Center, China Meteorological Administration, Beijing 100081, China

[4] School of Remote Sensing and Geomatics Engineering, Nanjing University of Information Science and Technology, Nanjing 210044, China

[5] Anhui Climate Center, Hefei 230031, China

[6] School of Earth and Space Sciences, University of Science and Technology of China, Hefei, Anhui 230026, China

Published online: 31 May 2018

daytime pollutants, the net effect of which is a slower cooling rate during the night in cities than in the suburbs, leading to a larger ΔT_{min}.

Keywords Beijing pollution · Fine particulate matter · $PM_{2.5}$ concentration · Urban heat island

1 Introduction

The urban heat island (UHI) is a microclimatic phenomenon caused by human activities and their effect on the land-surface temperature. The UHI phenomenon can be quantified using the UHI intensity, which is defined as the temperature difference between urban and rural areas, and is associated with many factors, such as the underlying surface roughness, surface albedo, and anthropogenic heating (Yang et al. 2013a, b; Li and Bouzeid 2014; Li et al. 2014; Ren 2015). Since Howard discovered the UHI effect in London (Howard 1883), a vast number of studies have been made to identify the causes of UHI effects, to understand the detailed spatial and temporal variations, and to quantify the impacts of the UHI effect on the surface energy balance, atmospheric boundary-layer structures, heatwaves, and precipitation processes (Weng and Yang 2004; Ren et al. 2007; Lin et al. 2008; Clinton and Gong 2013; Yang et al. 2013a, b; Li and Bouzeid 2013, 2014; Zhao et al. 2014).

The increase in local temperature resulting from the UHI effect can not only catalyze atmospheric photochemical reactions and lead to an increase in serious air pollution, but also induce the reproduction of microorganisms, such as bacteria and pathogens, and increase the speed of pathopoiesis (Stedman 2004; Anderson and Bell 2011). The importance of interactions between urban climates and biogeochemical cycles has been increasingly recognized, and thus the interactions have been the subject of many studies (Jacobson 1998; Crutzen 2004). Atmospheric particulate pollution is one of the major environmental factors endangering human health. Due to different underlying surface characteristics and differences in the fine-particle concentration and type between urban and rural areas, temperature changes resulting from aerosol-induced radiative forcing differ for urban and rural areas, which may further change the UHI intensity. While haze may intensify the UHI effect by absorbing solar radiation, aerosols may also cool the near-surface atmosphere by reflecting solar radiation. For instance, Zhang (2003) found that pollutants in the atmosphere have evident radiative effects, with a positive feedback between the atmospheric inversion layer and the warming effect of pollutants during the day through the absorption of solar radiation, which plays a leading role in the formation and development of the daytime atmospheric inversion layer. Zheng et al. (2006) noted that the longwave effect of aerosols at night may increase the near-ground temperature, but cool the low-level atmosphere. The shortwave effect of aerosols causes the near-surface layer to be significantly warmer during the daytime, leading to the enhancement of the UHI effect. Zhang et al. (2011) also found that aerosols over urban areas at night can weaken the upwards longwave radiation at the surface and slow down the cooling effect, which enhances the UHI effect. Based on model simulations, Miao et al. (2015a) noted that the surface net radiation and the sensible heat flux are reduced by aerosols by absorbing and scattering solar radiation in the atmosphere over Beijing, which increases the boundary-layer temperature, leading to a more stable and shallower boundary layer, giving higher $PM_{2.5}$ concentrations at the surface in the morning. Recently, Cao et al. (2016) attempted to isolate these conflicting effects with satellite observations and climate-model simulations, and estimated the corresponding relationship between pollutant concentrations

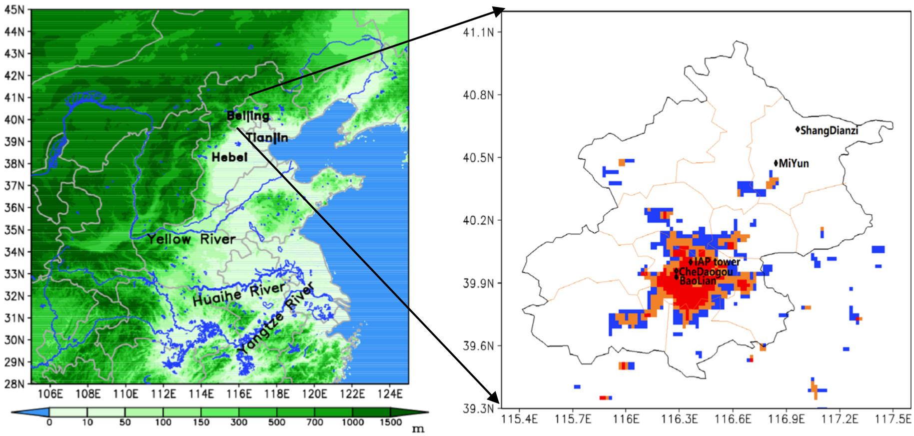

Fig. 1 Topography map of northern China and a map of observation-station locations in Beijing, whose basic information can be seen in Table 1 (red, yellow and blue colours indicate high-, middle- and low-population-density areas)

and UHI intensities in different cities in China. They found that, in more polluted areas, the UHI intensity is generally greater, with this phenomenon particularly evident in several semi-arid cities. Therefore, the relationship between fine-particle concentrations and the UHI intensity requires further investigation in megacities in China.

The Beijing–Tianjin–Hebei region is China's political, cultural and economic centre (Fig. 1). The atmospheric pollution level in Beijing, which is the region's largest and most important city, has continued to be high in recent years, with an elevated concentration in fine particulate matter (e.g., Zhao et al. 2014; Li et al. 2015; Lv et al. 2016; Miao et al. 2016). The problems associated with air pollution, such as the deterioration in human health and an increase in traffic, have caused a wide concern to both governmental departments and the public (An et al. 2007; Chen et al. 2013; San Martini et al. 2015). Extreme air-pollution incidents occur frequently in Beijing, and are linked not only to urbanization and emissions, but also to complex topographies and atmospheric circulations (Miao et al. 2014, 2015b, c). As rapid urbanization has significantly increased the UHI effect in Beijing (Liu et al. 2007; Ren et al. 2007; Yan et al.2010; Yang et al. 2013a), further investigation of the relationship between the UHI effect and fine-particle pollution must provide a practical reference for the establishment of optimal regional eco-environments. Because pseudo-correlated phenomena may occur, it is not possible to determine a credible causal relationship between these two factors when considering only a correlation coefficient. In this paper, the Granger causality method (Granger 1980) is used to analyze and test the relationship between fine particulate matter ($PM_{2.5}$) and UHI intensity in Beijing. Variations in hourly observed $PM_{2.5}$ concentrations at the surface are analyzed at different time scales, with the effects on UHI intensity also investigated in Beijing.

2 Data and Methods

2.1 Data

Unlike high-density, automatic-weather-station networks, air-quality observations are relatively sparse, and lack historical records over long periods. Here, $PM_{2.5}$ concentration data

Table 1 Basic information of observation stations

Station type	Station name	Elevation (m)	Observation
Urban	Baolian	55.8	$PM_{2.5}$
	Chedaogou	56	Air temperature at 2 m
	Institute of Atmospheric Physics Tower	49	Air temperature at 2 m, sensible and latent heat fluxes, turbulent kinetic energy
Rural	Miyun	73.4	Sensible and latent heat fluxes
	Shangdianzi	286.5	$PM_{2.5}$, air temperature at 2 m, radiation flux

from the Baolian and the Shangdianzi stations for 2012–2016 are presented (see Table 1 and Fig. 1). The two stations have been well maintained by the Beijing Environmental Meteorological Center, producing reliable observations with a 1400a-type tapered element oscillating microbalance manufactured by the R&P Corporation, USA, which measures $PM_{2.5}$ mass concentration at a temporal resolution of 1 h. Quality control was conducted to remove any unrealistic records. The Baolian station (39.90°N, 116.29°E) is located near the Beijing West Third Ring Road, which is used to represent the Beijing urban area. The Shangdianzi station (40.65°N, 117.10°E) is located approximately 130 km north-east of Beijing in Shangdian Village, Miyun County (see Fig. 1), and is the only regional atmospheric background station in North China. As pollution sources are lacking near this site, with its surrounding environment well protected and with little influence of urbanization, the Shangdianzi station can be used to represent the surrounding rural area of Beijing.

Since the Shangdianzi station is located near a mountainous area north-west of Beijing, the local topography may have an impact on the surrounding meteorological conditions, but the local-scale circulation is generally weak. For example, as the average mountain-valley wind speed in Beijing is <0.2 m s^{-1}, its impact on the multiyear average should not be significant (Zheng et al. 2018). More importantly, the Shangdianzi station has the longest observational period and the most rigorous observational quality compared with other rural stations. There are no continuous observational data of the same length in areas such as the southern plain of Beijing; even if observations were made there, the data would probably not be representative of the background due to the close proximity of major emission sources in Hebei Province. Based on these reasons, previous studies have also used the Shangdianzi station as a typical rural station to analyze the differences in urban and rural $PM_{2.5}$ concentrations (Miao et al. 2016).

Air-temperature data at 2 m above ground level with a temporal resolution of 1 h from automatic meteorological stations during the same period are available from the Beijing Meteorological Information Center, with the Chedaogou station selected for the urban area (see Table 1 and Fig. 1), which is 1.3 km north of the Baolian station, with similar surface conditions. For the rural area, the Shangdianzi station is used, which is located at an altitude of 286 m, and so the air temperature was adjusted to the same altitude as the Chedaogou station using a lapse rate of -0.65 K $(100\ m)^{-1}$ (Zheng et al. 2017). To investigate the effect of fine-particulate matter on the UHI effect, flux observations were used from the 325-m tower at the Institute of Atmospheric Physics (39.97°N, 116.37°E) and the Miyun weather station (40.36°N, 116.87°E), which are located in high- and low-density urban and rural areas in and outside Beijing, respectively (see Fig. 1 and Table 1).

Satellite-estimated radiation datasets are from the Clouds and Earth's Radiant Energy System (CERES) on board the Terra and Aqua satellites, and have been widely used in various applications (Yan et al. 2011; Pan et al. 2015). Here, the CERES_SYN1deg_Ed3A dataset (with a spatial resolution of $1° \times 1°$) available at http://ceres.larc.nasa.gov/order_data.php was used to provide upwards/downwards longwave and shortwave radiation fluxes under all-sky conditions. Radiation fluxes at the urban/rural sites were calculated by values available from the CERES grid closest to the site.

2.2 Methods

In climate analysis and research, several causal or physical connections between two variables are generally assumed when their correlation coefficient reaches a certain significance level. However, this assumption may imply a pseudo-correlation because self-correlation in a data sequence can affect the cross-correlation of different data sequences (Joliffe 1983). In recent years, significant advancement has been made in the study of climate-change detection and attribution, with several of such techniques developed from mathematical principles to identify the patterns of climate change (Houghton et al. 2001; Smith et al. 2003), and can generally be divided into two methods: the multiple-analysis method and the Bayesian-inference method. As the Bayesian-inference method can incorporate different sources of data, it receives more attention, but both methods still ignore self-variation when investigating the relationship between two variables.

As the Granger causality test considers not only the relationship between variables but also self-variations, it can effectively avoid the false-regression phenomenon, which gives it advantages in attribution analyses (Granger 1980). Granger's causal-analysis theory was first formulated by Clive W. J. Granger, and has become popular in economic analyses, signal processing and other fields for its simplicity and practicality. Cao et al. (2008) confirmed its usability in climatological studies, and further recommended it as a new method for climate-change detection and attribution analyses. Since then, the Granger causality test has been widely applied in climate-change research, such as climate-index attribution, urbanization effects, and temperature-trend analyses (Triacca 2001, 2005; Wang et al. 2004; Mosedale et al. 2006; Yu et al. 2016).

The Granger causality test is based on the fact that it does not necessarily ascertain a causal relationship between two variables (e.g., x and y) when the two variables are highly correlated, because the high correlation of x and y may be caused by a third factor; therefore, the causal relationship between x and y should be tested. The Granger causality test is a statistical-hypothesis test that determines whether one time series x is useful in forecasting another series y. First, we examine the extent to which the current value of y can be explained using a historical value of y; then, we investigate whether the interpretation can be improved by considering a lag value of x. The variable x is said to Granger-cause y if it can be shown that the x values provide statistically significant information regarding the potential values of y. The regression model is

$$\mathrm{x}_t = \sum_{i=1}^{n} \lambda_i x_{t-i} + \sum_{j=1}^{n} \mu_j y_{t-j} + u_{1t}, \tag{1}$$

$$\mathrm{y}_t = \sum_{i=1}^{m} \alpha_i y_{t-i} + \sum_{j=1}^{m} \beta_j x_{t-j} + u_{2t}, \tag{2}$$

where x_t and y_t represent two time series, u_{1t} and u_{2t} are theoretically uncorrelated error terms, and m and n indicate the order of the lags. The null hypotheses of Eqs. 1 and 2 are $\mu_1 = \mu_2 = \cdots = \mu_n = 0$ and $\beta_1 = \beta_2 = \cdots = \beta_m = 0$, respectively. If β_j is significantly unequal to zero, and μ_j is significantly equal to zero (in general), then it is believed that there is a single effect caused by x on y (i.e., x is the cause of the change in y), with the converse also true (i.e., y causes the change in$x$). In addition, there is a two-way causal relationship between x and y if both β_j and μ_j are significantly unequal to zero. The F-statistic

$$F = \frac{(SSE_r - SSE_u)/k}{SSE_u/(T - 2k)} \tag{3}$$

can be used for the above tests, where SSE_r represents the residual sum of squares when the null hypothesis is applied, whileSSE_u represents the residual sum of squares without any constraints, $k$indicates the maximum lag period, and T represents the sample size. We can calculate, with confidence, the probability using the p value from the F-statistic. For a given significance level α ($\alpha = 0.05$ here), if the p value is less than α, the null hypothesis is rejected, and x is said to Granger-cause y.

As stationarity of the original series is a prerequisite for the Granger causality test, which may otherwise lead to a false regression, a stationary test must be performed first, such as the augmented Dickey–Fuller test, which is a common method used to check the stationarity of a data series. The corresponding regression model is

$$\Delta x_t = \alpha + \beta_t + \rho x_{t-1} + \sum_{j=1}^{P} \lambda_j \Delta x_{t-j} + u_t, \tag{4}$$

where x_t represents the original sequence, x_{t-1} represents the original sequence with a lag of one timestep, Δx_t represents the first-order differenced sequence, Δx_{t-j} represents the first-order differenced sequence of j lag lengths, α is a constant term, with β_t, ρ and λ_j regression coefficients, P represents the lag length, and u_t is the error term. The null hypothesis of the augmented Dickey–Fuller test is $\rho = 0$, which means that the sequence has a unit root, and is thus non-stationary. If the null hypothesis is rejected, then the sequence is stationary. A non-stationary time sequence requires some transformation. Generally, a stationary sequence can be obtained by several differential transformations, which do not change the causal relationship between the original variables.

3 Results

3.1 Urban–Rural Difference in $PM_{2.5}$ Mass Concentration in Beijing

Figure 2 shows the 5-year interannual variation from 2012 to 2016 in $PM_{2.5}$ mass concentration at the Beijing Baolian urban and Shangdianzi rural sites, with average concentrations of $PM_{2.5}$ of 63.2 and 40.7 $\mu g\ m^{-3}$, respectively. While the Shangdianzi station is far away from the urban area, the air there is relatively clean, but the average annual $PM_{2.5}$ mass concentration is still higher than the national secondary standard (35 $\mu g\ m^{-3}$), with data from the urban station showing a worse air quality. In the most recent five years, due to the government's environmental protection policy, the $PM_{2.5}$ mass concentration in Beijing has steadily decreased, indicating that air quality is improving. In particular, as the decrease in $PM_{2.5}$ concentration in urban areas is more pronounced than in rural areas, the urban–rural $PM_{2.5}$ mass-concentration difference is gradually decreasing.

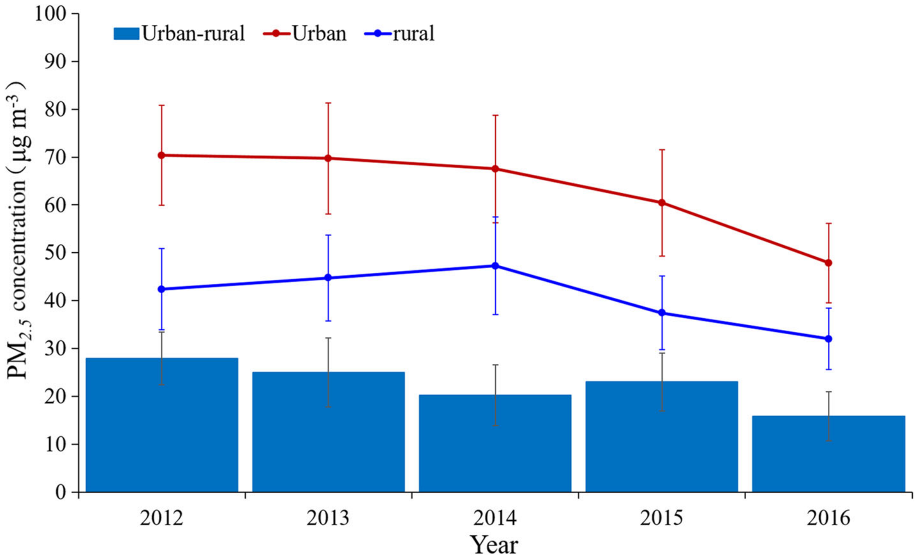

Fig. 2 Interannual variation of $PM_{2.5}$ mass concentration in the Beijing area

According to Cai et al. (2017), global warming has led to an increase in the occurrence of atmospheric stagnation in the North China Plain, and weather conditions have become increasingly conducive to haze formation. However, air quality has gradually improved even under such circumstances, which is related to the series of environmental protection measures taken by the local government. For example, Beijing started to limit the number of motorized vehicles in 2008, and began to control the increase in motor vehicles in 2011. In addition, the government has implemented stricter environmental policies with neighbouring provinces and municipalities since 2013, and emissions have decreased. Figure 3 presents the diurnal and monthly variations in $PM_{2.5}$ mass concentrations in the urban and rural areas of Beijing, indicating the $PM_{2.5}$ mass concentration for the urban area varies significantly throughout an average year. From the perspective of a seasonal variation, the highest and second highest $PM_{2.5}$ concentrations occur in winter and autumn, respectively, followed by spring and summer, but the $PM_{2.5}$ concentrations in autumn and winter are drastically higher. Specifically, the $PM_{2.5}$ mass concentration reaches its peak (> 80 $\mu g\ m^{-3}$) in December and January, with relatively lower values in the spring and summer months. For example, the mean value of $PM_{2.5}$ concentration in August is 42.1 $\mu g\ m^{-3}$, which is only approximately half of the peak annual value. According to previous studies (Miao et al. 2015d; San Martini et al. 2015;Tang et al. 2016; Li et al. 2017), the low concentration of $PM_{2.5}$ in spring is related to the large average wind speeds, and an increase in high-wind-speed days during the period, while low values in July, August and September primarily correspond to wet deposition resulting from summer precipitation.

Compared with urban areas, the seasonal variation in $PM_{2.5}$ concentration at the rural station is not as significant. The urban–rural difference in the $PM_{2.5}$ mass concentration is large in autumn and winter, amounting to 44 $\mu g\ m^{-3}$ in January, which is larger than the multiyear average (42.2 $\mu g\ m^{-3}$) in the rural area. During spring and summer, the urban–rural difference in the $PM_{2.5}$ mass concentration is small ($\approx$ 10 $\mu g\ m^{-3}$ in July, August and September). Such a variation is probably related to the excessive emission of pollutants in

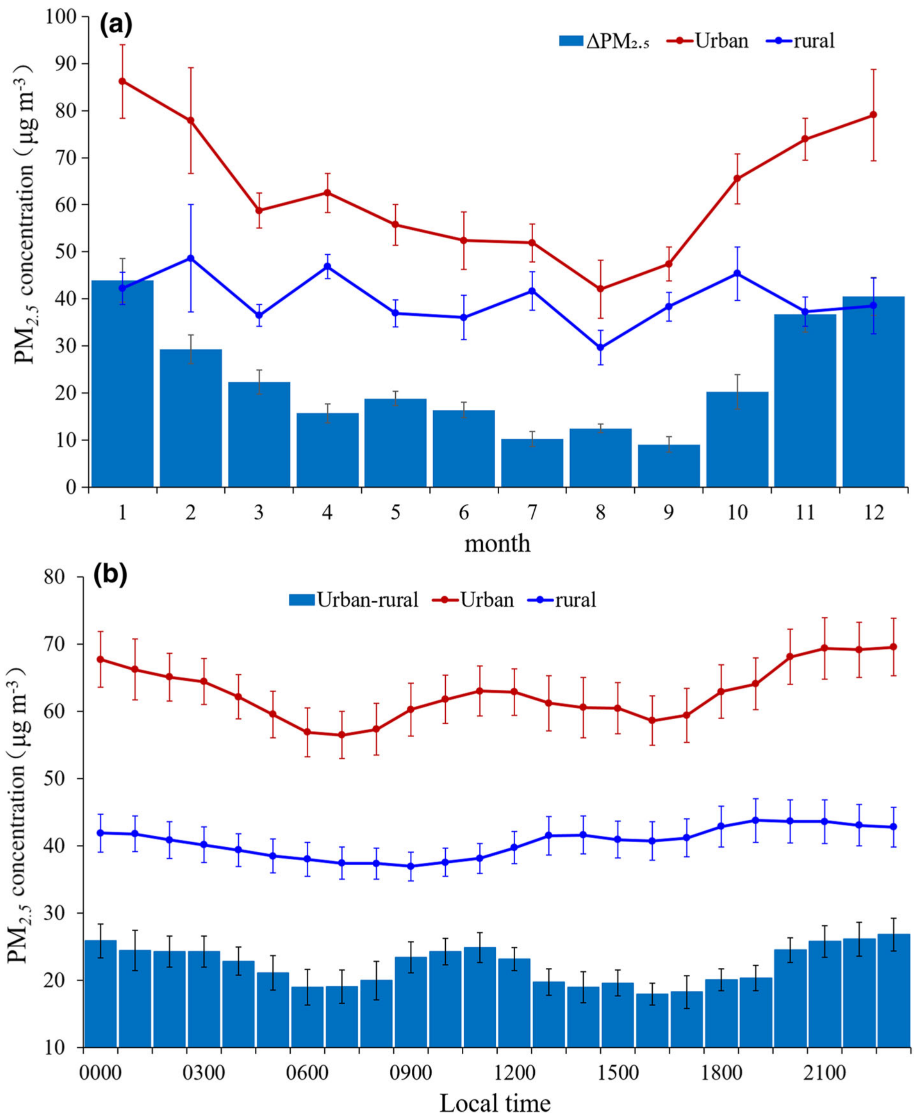

Fig. 3 **a** Monthly and daily variation **b** of $PM_{2.5}$ concentration in Beijing urban (brown line) and rural (blue line) areas, and the urban–rural $PM_{2.5}$ concentration difference (blue bars)

populated urban areas during the heating season (which usually begins 15 November and ends 15 March of the following year). In addition, the stable atmospheric circulation in autumn and winter makes it more difficult for the diffusion of pollutants. However, during summer, the boundary-layer height usually increases, and atmospheric conditions enable the enhanced diffusion of pollutants compared with that in winter, which may contribute to the reduced urban–rural difference in the $PM_{2.5}$ mass concentration in summer (Miao et al. 2015d). The difference in the seasonal variations in $PM_{2.5}$ can be explained by autumn and winter being traditional heating and coal-burning seasons in northern China. In urban areas, the concentrations of $PM_{2.5}$ in autumn and winter are relatively high because of the concentrated population and the resulting increased energy consumption, while the heating energy consumption is lower in rural areas because of a smaller population.

The average temporal variation in the $PM_{2.5}$ concentration at the urban station from 2012 to 2016 behaves in a semi-diurnal manner (Fig. 3b), with the first daily minimum appearing at 0600–0700 local time (LT), and the first concentration maximum at 1100 LT, before decreasing to a minimum at approximately 1600 LT, and reaching the second maximum at 2300 LT. Such a trend is consistent with previous studies on Beijing and other cities, and corresponds to the daily variation in anthropogenic activities, as well as to turbulence in the atmospheric boundary layer (Miao et al. 2015a). In contrast, the average hourly $PM_{2.5}$ concentration at the rural station is significantly lower than that in the urban area, indicating a diurnal variation with a single peak. In contrast to the urban area, the rural area has the lowest concentration at 0900 LT, which increases from 0900 to 1300 LT before levelling off from 1400 to 1600 LT, and then increasing after 1600 LT, and reaching a maximum at 1900 LT. The evolution of the $PM_{2.5}$ concentration at the rural station at night is similar to that at the urban station.

According to previous research (e.g., San Martini et al. 2015; Tang et al. 2016), the semi-diurnal variations in PM concentration at different cities during different seasons may result from different atmospheric diffusion conditions, which are related to various geographical and meteorological factors, as well as the different emission sources, with the semi-diurnal variation in the $PM_{2.5}$ concentration in Beijing likely the result of the following factors. The first peak in $PM_{2.5}$ concentration in the urban area during the daytime is related to the morning rush hour corresponding to the increase in the number of vehicles and emissions from factories. The second peak at night is related to the increased number of vehicles after work, large trucks entering the city at night, as well as the diurnal variations in meteorological conditions (i.e., reduced boundary-layer height and weaker turbulence) and chemical-reaction intensity, which are conducive conditions to the accumulation and secondary generation of urban $PM_{2.5}$, respectively. Due to reduced anthropogenic activities in rural areas, the concentration of $PM_{2.5}$ in the daytime fluctuates slightly because of mainly turbulent transport. Compared with the daytime peak in urban areas, the concentration increases significantly from the morning until late afternoon, with a peak at approximately 1900 LT.

3.2 The Correlation Between the Urban–Rural Difference in $PM_{2.5}$ Mass Concentration and Urban-Heat-Island Intensity

Figure 4 shows the monthly mean urban–rural difference in $PM_{2.5}$ mass concentration $\Delta PM_{2.5}$ and the UHI intensity ΔT in the Beijing area from 2012 to 2016, indicating a consistent correlation between the two variables at the monthly scale. For example, $\Delta PM_{2.5}$ and ΔT values are both larger in autumn and winter and smaller in spring and summer. However, a high monthly $\Delta PM_{2.5}$ value does not necessarily correspond to a high monthly ΔT value. For example, the magnitude of $\Delta PM_{2.5}$ is larger in January than in December, while the magnitude of ΔT is not, with a similar pattern also occurring in April and September. The discrepancy at the monthly scale indicates that $\Delta PM_{2.5}$ and ΔT values can vary asynchronously due to other factors, including the impacts of local synoptic processes and temporary government restrictions.

Some studies have shown that the UHI effect on metropolitan areas has an obvious asymmetry for different temperature indexes: the UHI effect on the daily minimum temperature (daily maximum temperature) is the strongest (weakest), with the UHI effect having an intermediate impact on the daily mean temperature (Liu et al. 2007; Yang et al. 2013a, b). In

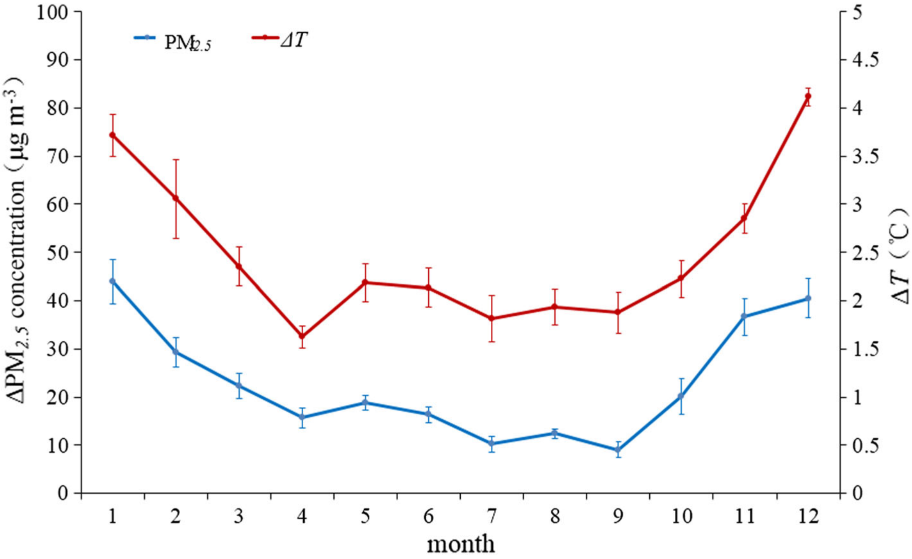

Fig. 4 The monthly mean urban–rural difference of $PM_{2.5}$ mass concentration ($\Delta PM_{2.5}$) and the UHI intensity ΔT in the Beijing area

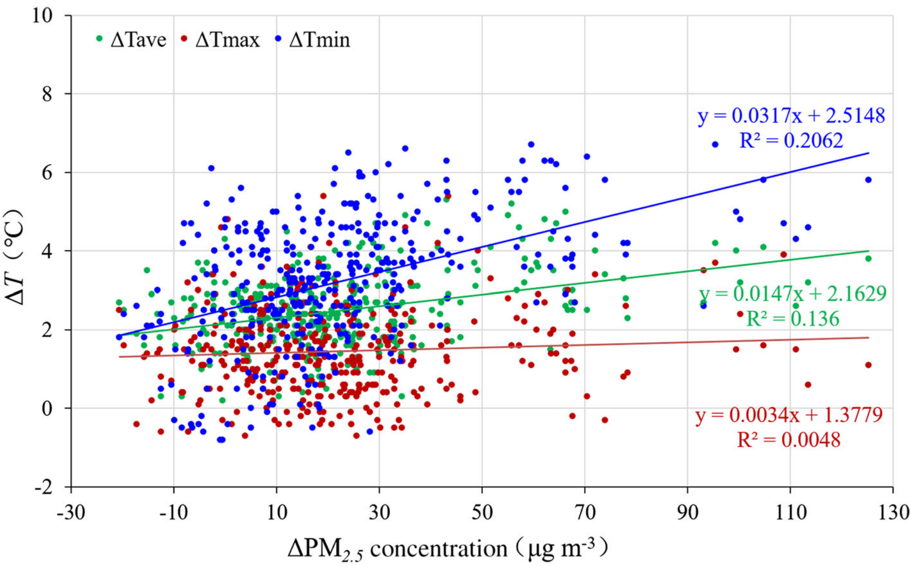

Fig. 5 The daily-averaged $\Delta PM_{2.5}$ and ΔT_{ave} (daily-averaged temperature difference between the urban and rural areas), ΔT_{max} (daily-maximum temperature difference between the urban and rural areas), and ΔT_{min} values (daily-minimum temperature difference between the urban and rural areas)

addition, there are significant diurnal and seasonal variations in the UHI intensity (Liu et al. 2007; Yang et al. 2013a). Figure 5 shows the correlation between daily mean $\Delta PM_{2.5}$ and ΔT_{ave} (i.e., the daily average temperature difference between urban and rural areas), ΔT_{max} (i.e., the daily maximum temperature difference between urban and rural areas) and ΔT_{min}

Table 2 The correlation coefficient between $\Delta PM_{2.5}$ and ΔT values (* represents significance at the 0.01 level)

$\Delta PM_{2.5}$	The same day					Lag of 1 day	Lag of 2 days	Lag of 3 days
	Annual	Spring	Summer	Autumn	Winter			
ΔT_{ave}	0.087	0.304*	0.109	0.270*	0.344*	0.310*	0.251*	0.205*
ΔT_{min}	0.454*	0.304*	0.342*	0.362*	0.378*	0.314*	0.302*	0.265*
ΔT_{max}	0.069	0.100	0.059	0.010	0.090	0.054	0.084	0.157*

values (i.e., the daily minimum temperature difference between urban and rural areas), indicating the largest correlation coefficient (0.45) between the daily mean $\Delta PM_{2.5}$ and ΔT_{min} values, followed by the correlation coefficient between the daily mean $\Delta PM_{2.5}$ and ΔT_{ave} of 0.37, while the correlation coefficient between the daily mean $\Delta PM_{2.5}$ concentration and ΔT_{max} values is only 0.07. For the winter season, the correlation coefficient between the $\Delta PM_{2.5}$ concentration and the UHI intensity is the highest, resulting in correlation coefficients of 0.38, 0.34 and 0.09 for ΔT_{min}, ΔT_{ave} and ΔT_{max}, respectively. The correlation coefficient between the $\Delta PM_{2.5}$ concentration and the UHI intensity is lowest during spring.

Previous studies have also indicated a relationship between the $PM_{2.5}$ mass concentration in urban areas and the UHI intensity, such as that by Wu et al. (2014). Here, we also calculated and obtained correlation coefficients between the $PM_{2.5}$ concentration in urban areas and ΔT_{ave}, ΔT_{max} and ΔT_{min} values in the Beijing area of 0.24, 0.04 and 0.33, respectively, which are smaller than those between $\Delta PM_{2.5}$ and ΔT_{ave}, ΔT_{max} and ΔT_{min}, implying that $\Delta PM_{2.5}$ is more closely related to the UHI intensity. Further analysis shows that the above correlation between $\Delta PM_{2.5}$ and ΔT values is statistically significant (Table 2), with the correlations between $\Delta PM_{2.5}$ and ΔT_{ave} and between $\Delta PM_{2.5}$ and ΔT_{min} significant at the 0.01 level (for a total sample size of 365). Introducing lags of 1–3 days (i.e., ΔT of 1, 2 and 3 days after the $\Delta PM_{2.5}$ observation) gives correlations still generally significant at the 0.01 level, although the degree of correlation is slightly lower. Considering the values of these correlation coefficients, $\Delta PM_{2.5}$ and ΔT_{min} (ΔT_{max}) have the strongest (weakest) correlation.

3.3 Granger Causality Test

3.3.1 Stationarity Analysis

Granger causality theory requires that a given variable be stationary for causality testing because non-stationary signals may introduce a pseudo-regression into the Granger causality test, which may lead to erroneous conclusions. Therefore, the stationarity of the time series should be confirmed before the Granger causality test. If the variable is found to be non-stationary, it may be either transformed differentially or logarithmically until the variable becomes stationary. The stationarity of the sequences analyzed using the augmented Dickey–Fuller test indicate unit-root values for $\Delta PM_{2.5}$, ΔT_{ave}, ΔT_{max} and ΔT_{min} of -5.91, -4.00, -8.97 and -5.03, respectively, which are all less than the 0.01 standard confidence level (-3.45), implying the data are all stationary, and can be directly used in the Granger causality test.

3.3.2 The Granger Causality Test

Table 3 shows the results of the Granger causality test between $\Delta PM_{2.5}$ and ΔT values (including ΔT_{ave}, ΔT_{min} and ΔT_{max}) for a significance level α of 0.05 (i.e., the fiducial probability is 95%). For $k=1$ (i.e., ΔT lags $\Delta PM_{2.5}$ by 1 day when considering $\Delta PM_{2.5}$ as the cause, and $\Delta PM_{2.5}$ lags ΔT by 1 day when considering ΔT as the cause), the results

Table 3 Granger causality test results; N is the sample size, F is the F-statistic of the Granger causality test, and p is the confidence probability; $k=1$, 2 or 3 implies ΔT lags of 1, 2 or 3 days, respectively, of $\Delta PM_{2.5}$ when considering $\Delta PM_{2.5}$ as the cause, and $\Delta PM_{2.5}$ lags of 1, 2 or 3 days, respectively, of ΔT values when considering ΔT as the cause

Lag	Hypothesis	N	F	p
k = 1	**$\Delta PM_{2.5}$ is not the Granger cause of ΔT_{ave}**	**364**	**3.91278**	**0.0487**
	ΔT_{ave} is not the Granger cause of $\Delta PM_{2.5}$	**364**	**23.6529**	**2.E−06**
	$\Delta PM_{2.5}$ is not the Granger cause of ΔT_{max}	364	0.67996	0.4101
	ΔT_{max} is not the Granger cause of $\Delta PM_{2.5}$	364	0.00993	0.9207
	$\Delta PM_{2.5}$ is not the Granger cause of ΔT_{min}	**364**	**14.9142**	**0.0001**
	ΔT_{min} is not the Granger cause of $\Delta PM_{2.5}$	**364**	**6.34368**	**0.0122**
$k=2$	**$\Delta PM_{2.5}$ is not the Granger cause of ΔT_{ave}**	**363**	**12.0002**	**9.E−06**
	ΔT_{ave} is not the Granger cause of $\Delta PM_{2.5}$	363	2.04581	0.1308
	$\Delta PM_{2.5}$ is not the Granger cause of $\Delta T\text{-}_{max}$	363	0.99208	0.3718
	ΔT_{max} is not the Granger cause of $\Delta PM_{2.5}$	363	0.15942	0.8527
	$\Delta PM_{2.5}$ is not the Granger cause of ΔT_{min}	**363**	**4.97259**	**0.0074**
	ΔT_{min} is not the Granger cause of $\Delta PM_{2.5}$	**363**	**5.46383**	**0.0046**
$k=3$	**$\Delta PM_{2.5}$ is not the Granger cause of ΔT_{ave}**	**362**	**7.61373**	**6.E−05**
	ΔT_{ave} is not the Granger cause of $\Delta PM_{2.5}$	362	0.77860	0.5065
	$\Delta PM_{2.5}$ is not the Granger cause of ΔT_{max}	362	2.51571	0.0581
	ΔT_{max} is not the Granger cause of $\Delta PM_{2.5}$	362	0.44699	0.7196
	$\Delta PM_{2.5}$ is not the Granger cause of ΔT_{min}	**362**	**3.86337**	**0.0097**
	ΔT_{min} is not the Granger cause of $\Delta PM_{2.5}$	362	2.48372	0.0606

Bold lines represent the rejection of the null hypothesis reject the null hypothesis of $\Delta T_{ave}/\Delta T_{min}$ with a probability of $p<0.05$, which leads to the conclusion that there is a two-way causal relationship between $\Delta PM_{2.5}$ and $\Delta T_{ave}/\Delta T_{min}$ values. However, there is no Granger causality between $\Delta PM_{2.5}$ and ΔT_{max} values, since the corresponding p value is >0.05.

For $k=2$, there is a mutual Granger causality relationship between $\Delta PM_{2.5}$ and ΔT_{min} values, which means that $\Delta PM_{2.5}$ and ΔT_{min} values can influence each other over the course of two days. Furthermore, $\Delta PM_{2.5}$ is still the Granger cause of ΔT_{ave} values, indicating that the $\Delta PM_{2.5}$ concentration has a significant effect on the ΔT_{ave} value of the following day, but the opposite is not true. For ΔT_{max} values, as mentioned previously, the results do not show any Granger causality with the $\Delta PM_{2.5}$ concentration.

For $k=3$, the test results show that $\Delta PM_{2.5}$ is still a Granger cause of ΔT_{min} and ΔT_{ave} values, while both ΔT_{min} and ΔT_{ave} values are no longer Granger causes of the $\Delta PM_{2.5}$ concentration, which cannot be inferred through the correlation coefficients in Table 2. In contrast, ΔT_{max} values and the $\Delta PM_{2.5}$ concentration are still not associated directly.

Overall, the results show that there is a possible causal relationship and positive feedback between $\Delta PM_{2.5}$ and ΔT_{min} values, since they exhibit mutual causation, and can affect each other for lag periods within two days. Moreover, as the effect of $\Delta PM_{2.5}$ on ΔT_{min} values can last for approximately three days, the $\Delta PM_{2.5}$ concentration is probably the main cause of the UHI phenomenon, and the UHI effect may further enhance the $\Delta PM_{2.5}$ level.

3.4 Case Analysis

Figure 6 shows a heavy-pollution event in November 2015 in Beijing. During the day on 26 November, the $PM_{2.5}$ mass concentrations in the urban and rural areas were both very low. Following the night of 26 November, there was a rapid deterioration in air quality, and the rate of increase in the urban $PM_{2.5}$ mass concentration was significantly greater than that in the rural area. On the afternoon of 27 November, the urban $PM_{2.5}$ mass concentration exceeded 200 $\mu g\ m^{-3}$, with a maximum close to 300 $\mu g\ m^{-3}$, and the $PM_{2.5}$ mass-concentration difference between urban and rural areas was >150 $\mu g\ m^{-3}$. The temperature observed from the automatic weather station showed that, from 26–27 November, the diurnal cycle for temperature became weak corresponding to an increase in the $PM_{2.5}$ mass concentration, especially in urban areas. The UHI intensity became weaker (stronger) during the day (night), with ΔT_{max} (ΔT_{min}) = 2.9 °C (4.4 °C) on the 26 November, and − 1.1 °C (4.6 °C) on 27 November.

The increase in the concentration of fine particulate matter first caused the surface radiation flux to change. Table 4 shows the four CERES-based radiation values at the surfaces of the urban areas (near the Institute of Atmospheric Physics station) and the rural areas (near the Miyun station) from the 26–27 November 2015, indicating the downwards shortwave radiation reaching the surface decreased with an increase in the $PM_{2.5}$ concentration. The average downwards shortwave flux at the three stations on 26 November was 114 W m^{-2}, which decreased to 99 W m^{-2} on 27 November, with the decrease in downwards shortwave flux greater in urban areas than that in rural areas. The average upwards shortwave flux also decreased by approximately 4.5 W m^{-2}. At night, the presence of pollutants increased the longwave radiation reaching the surface and the atmosphere. From 26–27 November, the downwards longwave flux increased from 228 to 261 W m^{-2}, and was greater in urban areas than in rural areas. At the same time, the average upwards longwave flux increased by approximately 28 W m^{-2}. The effect of particulate matter on longwave and shortwave radiation was reduced from the urban to the rural areas, which is consistent with the distribution of pollutants. The above results are consistent with those in previous works (e.g., Wang et al.

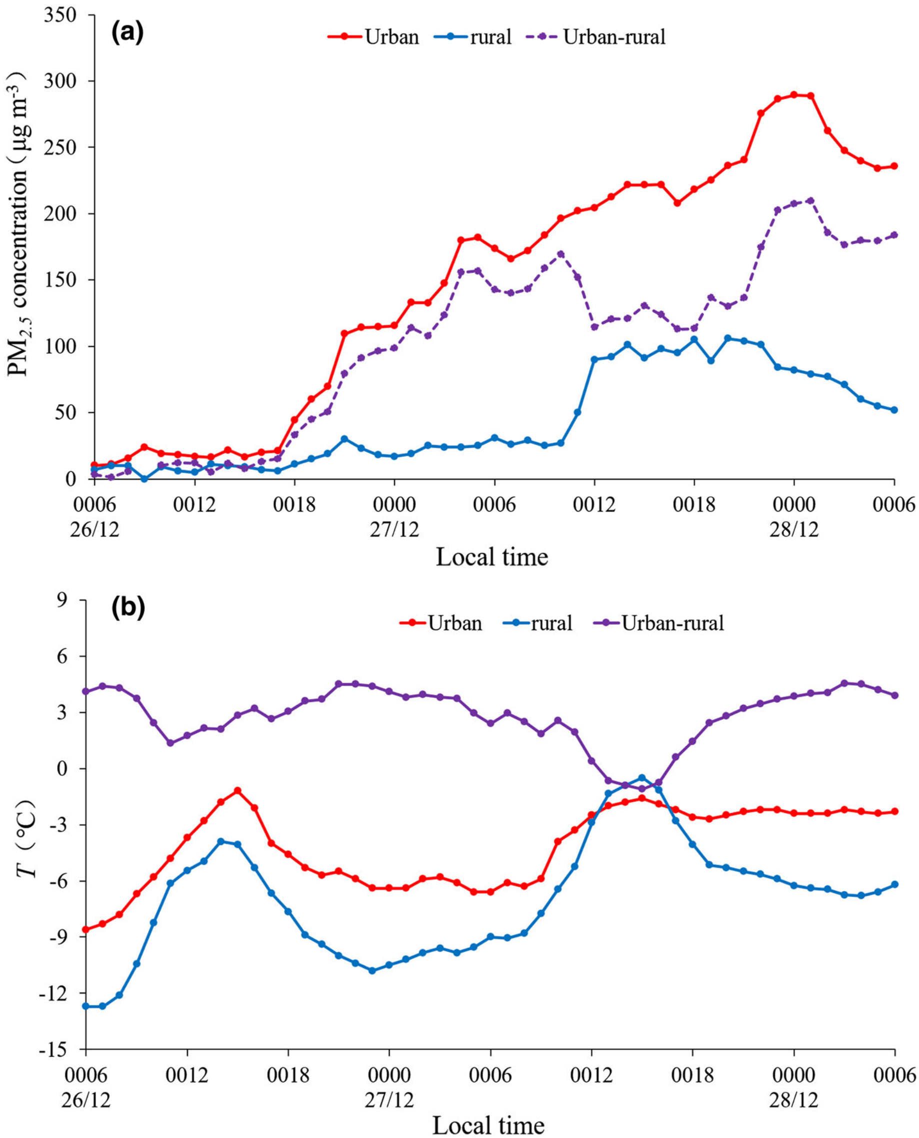

Fig. 6 The hourly **a** $PM_{2.5}$ concentration and **b** temperature observations from 26–28 November 2015

2016). While the variations in longwave radiation may be caused by water vapour, fog and clouds, both fog and haze are often associated with high $PM_{2.5}$ concentrations in Beijing. In this case, the meteorological observations show that the total cloud cover in Beijing on 26 November 2015 was 20%. The concentration of pollutants increased significantly on 27 November, with a total cloud cover of 50%, so that observed increase in cloud cover was likely caused by the increase in haze (Tan et al. 2017). From 26–27 November, the average relative humidity in urban areas was 45% and 53%, respectively, with the increase in relative humidity also consistent with the increase in $PM_{2.5}$ concentration.

Table 4 The CERES-based upwards shortwave flux, downwards shortwave flux, upwards longwave flux, and downwards longwave flux at the surface on 26 and 27 November 2015 at the urban Institute of Atmospheric Physics and rural Miyun stations and their differences between these two days

Station type	Date	Downwards shortwave flux (W m^{-2})	Upwards shortwave flux (W m^{-2})	Downwards longwave flux (W m^{-2})	Upwards longwave flux (W m^{-2})
Urban	26 November 2015	114.3	28.7	246.1	260.9
	26 November 2015	98.6	24.6	286.3	286.3
	Difference	− 15.7	− 4.10	40.2	25.4
Rural	26 November 2015	113.6	25.9	210.5	248.9
	26 November 2015	99.6	20.8	236.4	278.6
	Difference	− 14.0	− 5.1	25.9	29.7

To further explore the effect of fine particulate matter on the surface energy budget, Fig. 7 shows the hourly variations in sensible and latent heat fluxes over urban (Institute of Atmospheric Physics station) and rural areas (Miyun station) from 26 to 28 November in 2015, indicating that, from 26 to 27 November, the downwards shortwave radiation reaching the ground in urban and rural areas decreased with an increase in $PM_{2.5}$ concentration (Table 4), which resulted in a decrease in the sensible heat flux (Fig. 7) and an attenuation of the warming of the near-surface atmosphere. For rural areas, the decrease in the sensible heat flux was not as obvious as that in urban areas due to the relatively small $PM_{2.5}$ mass concentration, and the warming of the near-surface atmosphere during the daytime was more rapid than that in urban areas, which led to a decrease in ΔT_{max} values (Fig. 6b). At night, the presence of fine particles can reduce the surface longwave flux and the latent heat flux, thus acting as an insulator. Because the $PM_{2.5}$ mass concentration in urban areas was larger than that in rural areas during this period, the insulation effect was large in urban areas, so that the temperature at night in the urban areas reduced more slowly than that in rural areas, with the value of ΔT_{min} maintained at a relatively high value.

4 Discussion

Previous studies have shown that average temporal variations in surface $PM_{2.5}$ concentrations in large- and medium-sized cities usually display bimodal or semi-diurnal characteristics (Xu et al. 2014; Zhao et al. 2014; Hu et al. 2014; Lv et al. 2016), with the two peaks corresponding to the morning and evening traffic peaks, while the concentrations in between these periods are lower. However, previous studies have also shown that, in different places or periods, various emission sources and meteorological conditions play important roles in shaping the temporal variation of $PM_{2.5}$ concentration (Li et al. 2015; Miao et al. 2017). For example, in a coastal city (e.g., Tianjin, China), the first peak can be delayed until noon, and the second peak can be postponed until midnight (Yao et al. 2010). However, the occurrences of maximum (1100 and 2300 LT) and minimum (0600–0700 and 1600 LT) $PM_{2.5}$ concentrations in Beijing are different in our results.

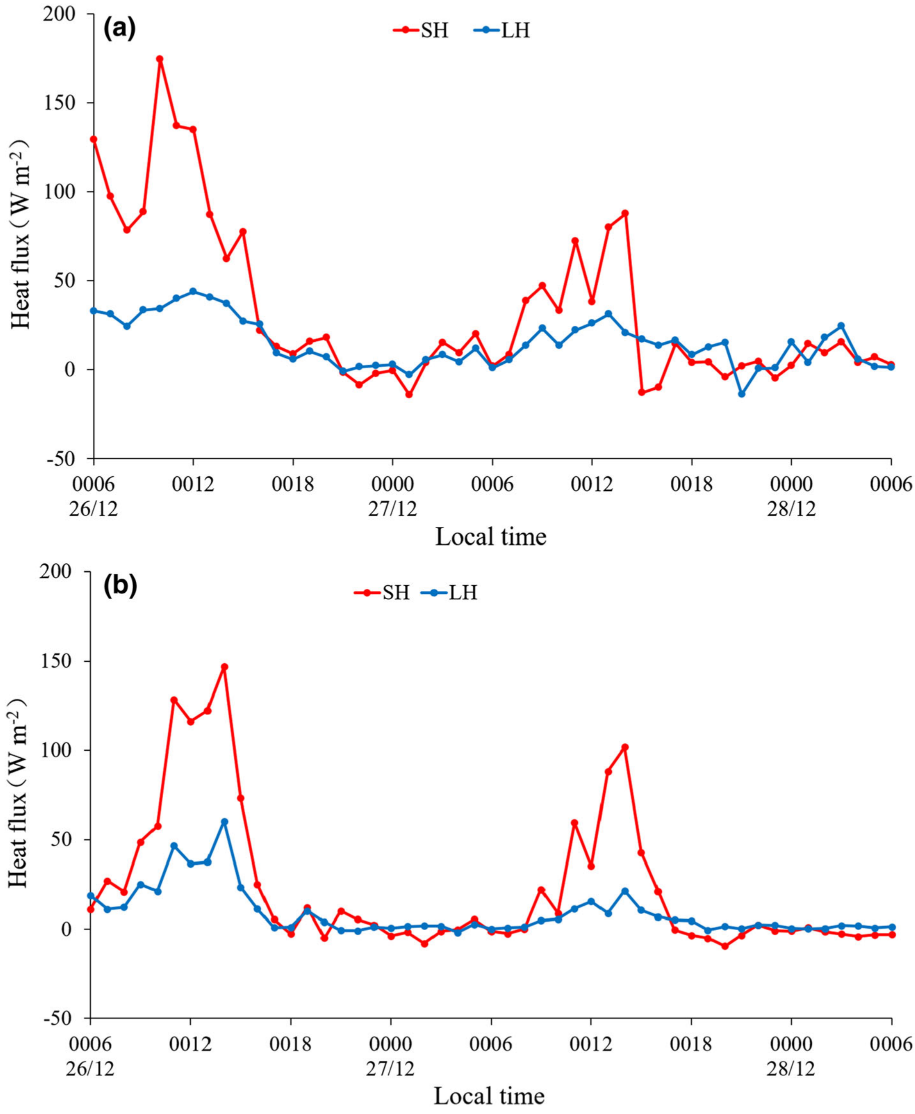

Fig. 7 The hourly sensible and latent heat fluxes from 26–28 November 2015 for **a** the urban Institute of Atmospheric Physics station, and **b** the rural Miyun station

The formation, maintenance and dissipation of pollutants are closely related to the meteorological conditions (Cai et al. 2017; Li et al. 2017; Miao et al. 2015a, 2017). For example, a high temperature or atmospheric inversion can exacerbate photochemical reactions, which favour the accumulation and secondary generation of $PM_{2.5}$. Meteorological conditions, such as static or small vertical transport, regional transport and unfavourable large-scale weather circulations (e.g., a uniform pressure field or high pressure at the surface) are not conducive to the dissipation of pollutants (Cai et al. 2017; Miao et al. 2017). The cross-regional transport of pollutants can even lead to an increase in the concentration of local particulate matter. At the urban scale, due to the complexity of boundary-layer structure and the local circulation in urban areas (i.e., due to the UHI–pollution interaction), there is a complex relationship between the UHI effect and fine-particle pollution. The increase in surface fine-particle concentrations generally fosters the formation of an inversion layer at night during autumn and winter (Miao et al. 2015a, d), resulting in stable atmospheric conditions, with the turbulent kinetic energy weakening with consistently steady weather (Fig. 8), which inhibits vertical diffusion and leads to the further accumulation of contaminants locally. From 26–27 November 2015, a strong inversion layer existed between the surface and 47-m height for most hours, and a strong inversion layer existed between the surface and 140-m height at night (see Fig. 8), which greatly weakened turbulence and the diffusion of pollutants. The effect of the UHI may also affect the distribution of fine particulate matter through UHI-induced circulations. Figure 6a shows that the $PM_{2.5}$ mass concentration during the night (from 2100 LT 26 November to 0100 LT 27 November, and from 2000 LT 27 November to 0600 LT 28 November) decreased in rural areas, but increased in urban areas, with similar variations also seen in Fig. 3b. This higher concentration of fine particles in urban areas is mainly related to the emission of pollutants and the reduced depth of the boundary layer, although there may still be a weak UHI circulation. Figure 9 shows the diurnal variations in the local wind field in Beijing for wind speeds averaged over the last eight years. The removal of the large-scale circulation background (Zheng et al. 2018) can effectively highlight local circulation characteristics in Beijing, which mainly show UHI circulations and mountain–valley flow circulations. By comparing Fig. 3b with Fig. 9, a good relationship can be seen between the diurnal variation in $PM_{2.5}$ concentrations in Beijing urban areas and the local flow field, suggesting that, from the afternoon to the middle of the night, southerly local flow tends to transport foreign pollutants into the urban areas of Beijing. The obstruction of the western and northern mountains further contributes to the accumulation of pollutants, increasing the concentration of pollutants starting in the afternoon. Therefore, it is possible that, especially for the night, the weak near-ground convergence of local UHI circulation combined with the mountain-valley breeze transports fine particles from rural areas back towards urban areas (Liu et al. 2009), which leads to the accumulation of pollutants in urban areas. This indicates a positive feedback due to the interaction between air pollutants and the UHI effect.

It should be noted that there are uncertainties regarding the impact of particulate matter on the UHI effect due to uncertainties in geographical factors and research methods. For example, in different cities, the pollution source or its geographical characteristics may differ, leading to drastically different particle sizes (Zhao et al. 2013). Previous studies have indicated that particles with different sizes have different effects on longwave and shortwave radiation (e.g., Cao et al. 2016). A detailed analysis is planned using a high-resolution numerical model and observations.

5 Summary

The characteristics of surface $PM_{2.5}$ mass concentrations in the Beijing area and the relationship with the UHI effect were analyzed by using observational data from 2012 to 2016. The main conclusions are as follows:

1. The 5-year-average surface concentrations of $PM_{2.5}$ in the Beijing urban and rural areas are 63 and 41 $\mu g\ m^{-3}$, respectively, and the annual averages in these two areas have both decreased. In urban areas, the surface $PM_{2.5}$ concentrations have significant interannual

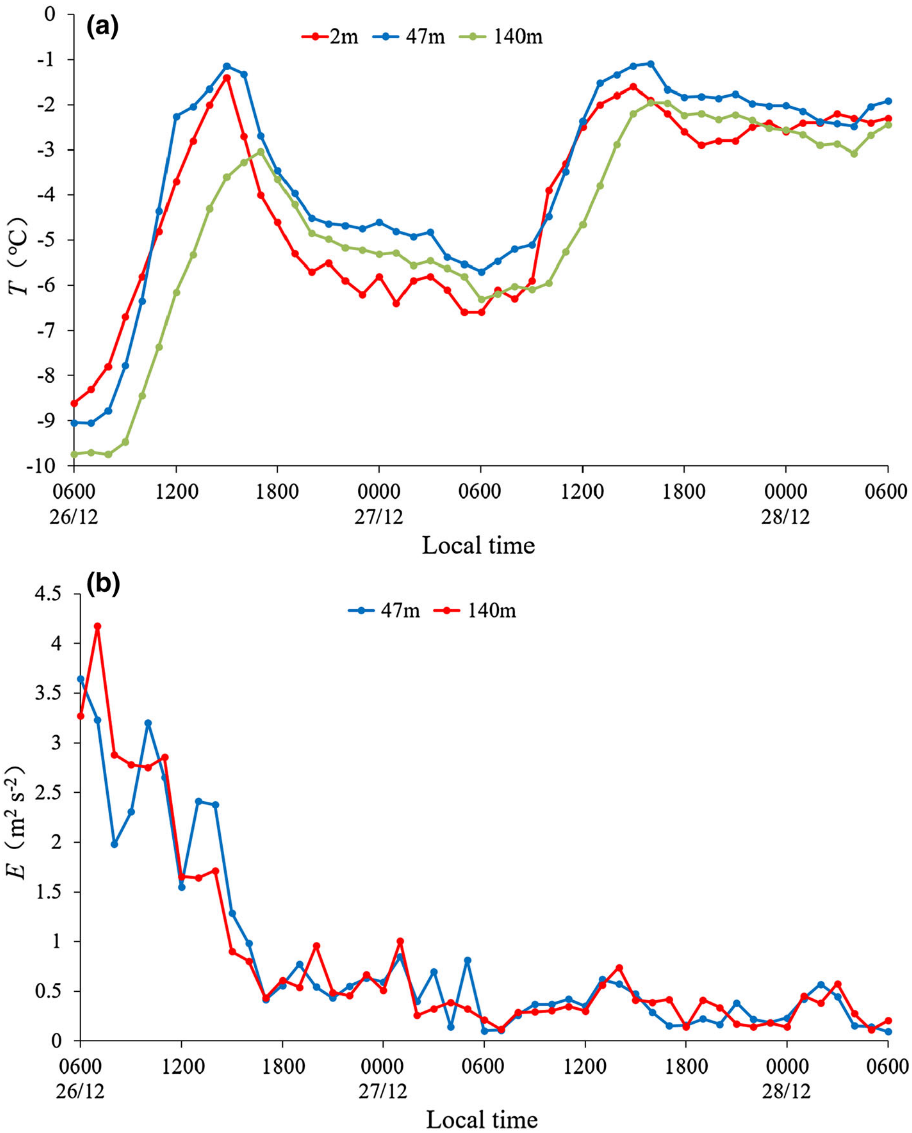

Fig. 8 Hourly **a** air temperature and **b** turbulent kinetic energy (E) from 26–28 November 2015, which is the local time

and seasonal variations and a semi-diurnal cycle. In rural areas, the interannual variation is not evident, with the diurnal cycle featuring a single peak concentration.

2. There is a strong correlation between $\Delta PM_{2.5}$ (urban–rural $PM_{2.5}$ concentration) and UHI intensity ΔT. Specifically, the correlation between $\Delta PM_{2.5}$ and ΔT_{min} values is the highest, followed by the correlation between $\Delta PM_{2.5}$ and ΔT_{ave} values, with the correlation between $\Delta PM_{2.5}$ and ΔT_{max} values the lowest. From a seasonal perspective, the correlation between $\Delta PM_{2.5}$ and ΔT values in winter is the strongest.
3. Granger's causality analysis shows that the relationship between $\Delta PM_{2.5}$ and ΔT_{min} values is the strongest; ΔT_{min} may affect $\Delta PM_{2.5}$ over the course of two days, while $\Delta PM_{2.5}$

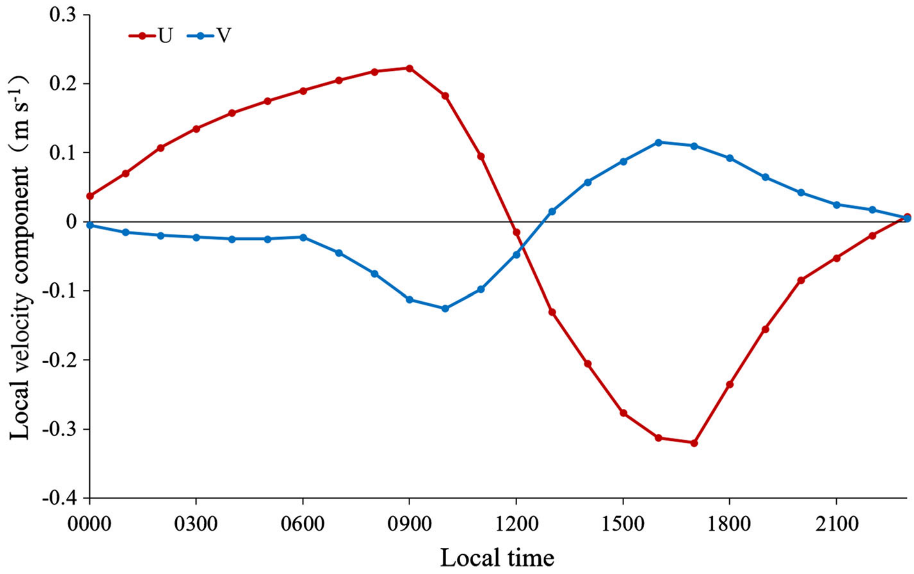

Fig. 9 Diurnal variations of the local wind-speed anomaly based on eight years of observations in Beijing; *U* indicates the east–west velocity component (positive value: eastwards), *V* indicates the north–south velocity component (positive value: northwards)

may affect ΔT_{min} over the course of three days. The relationship between $\Delta PM_{2.5}$ and ΔT_{ave} is moderate, and these two variables have a mutual causal relationship after one day. Granger's causality test shows that there is no causal relationship between $\Delta PM_{2.5}$ and ΔT_{max} values.

4. The case analysis shows that, with an increase in surface $PM_{2.5}$ concentration, the downwards shortwave radiation at the surface decreases during the daytime, which mitigates the warming of the atmosphere. At night, fine particles reduce the loss of longwave radiation from the surface, maintaining urban areas warmer than rural areas, leading to an increased value of ΔT_{min}, which indicates that the longwave radiation from the surface is weaker on polluted days than on relatively clean days.

Acknowledgements This study is supported by National Key Research and Development Program of China (2016YFC0203300) the National Natural Science Foundation of China (41575010, 41575003, 41601550, 41505004, and 41675009), National special project for international scientific and technological cooperation (2015DFA20870) National Key, and the CMA climate change special foundation (CCSF201726).

References

An X, Tong Z, Wang ZF, Li C, Wang Y (2007) A modeling analysis of a heavy air pollution episode occurred in Beijing. Atmos Chem Phys 7(12):3103–3114

Anderson GB, Bell ML (2011) Heat waves in the United States: mortality risk during heat waves and effect modification by heat wave characteristics in 43 U.S. communities. Environ Health Persp 119(2):210–218

Cai WJ, Li k, Liao H, Wang HJ, Wu LX (2017) Weather conditions conducive to Beijing severe haze more frequent under climate change. Nat Clim Change 4:257–262

Cao HX, Zheng Y, Yu HY, Cai XH (2008) Granger causality test for detection and attribution of climate change. Adv Clim Change Res 4(1):14–37 **(in Chinese)**

Cao C, Lee X, Liu SD, Schultz N, Xiao W, Zhang M, Zhao L (2016) Urban heat islands in China enhanced by haze pollution. Nat Commun. https://doi.org/10.1038/ncomms12509

Chen YY, Ebenstein A, Greenstone M, Li HB (2013) Evidence on the impact of sustained exposure to air pollution on life expectancy from China's Huai River policy. Proc Natl Acad Sci USA 110:12936–12941

Clinton N, Gong P (2013) MODIS detected surface urban heat islands and sinks: global locations and controls. Remote Sens Environ 134:294–304

Crutzen PJ (2004) New Directions: The growing urban heat and pollution "island" effect impact on chemistry and climate. Atmos Environ 38:3539–3540

Granger (1980) Testing for causality: a personal view point. J Econ Dyn Control 2:329–352

Houghton JT, Ding Y, Griggs DG (2001) Climate change 2001: the scientific basis. Contribution of working group I to the third assessment report of the IPCC. Cambridge University Press, Cambridge

Howard L (1883) The climate of London deduced from meteorological observation, 3rd ed, vol 1. Harvey and Darton, London, 348 pp

Hu JL, Wang YG, Ying Q, Zhang HL (2014) Spatial and temporal variability of PM2.5 and PM10 over the North China Plain and the Yangtze River Delta China. Atmos Environ 95:598–609

Jacobson MZ (1998) Studying the effects of aerosols on vertical photolysis rate coefficient and temperature profiles over an urban airshed. J Geophys Res 103:10593–10604

Joliffe IT (1983) Why do we get spurious correlation in climatology: some explanations. II Int Meet Stat Climatol 16(4):1–6

Li D, Bouzeid E (2013) Synergistic interaction between urban heat islands and heat waves: the impact in cities is larger than the sum of its parts. J Appl Meteorol Climatol 52:2051–2064

Li D, Bouzeid E (2014) Quality and sensitivity of high-resolution numerical simulation of urban heat islands. Environ Res Lett 9:055001

Li D, Bouzeid E, Oppenheimer M (2014) The effectiveness of cool and green roofs as urban heat island mitigation strategies. Environ Res Lett 9:055002

Li RK, Li ZP, Gao WJ, Ding WJ, Xu Q, Song XF (2015) Diurnal, seasonal, and spatial variation of PM2.5 in Beijing. Sci Bull 60(3):387–395

Li XL, Ma YJ, Wang YF, Liu NW, Hong Y (2017) Temporal and spatial analyses of particulate matter (PM10 and PM2.5) and its relationship with meteorological parameters over an urban city in northeast China. Atmos Res 198:185–193

Lin CY, Chen F, Huang JC, Chen WC, Liu YA, Chen WN, Liu SC (2008) Urban heat island effect and its impact on boundary layer development and land-sea circulation over northern Taiwan. Atmos Environ 42(22):5635–5649

Liu W, Ji C, Zhong J, Jiang X, Zheng Z (2007) Temporal characteristics of the Beijing urban heat island. Theor Appl Climatol 87(4):213–221

Liu SH, Liu ZX, Li J, Wang YC, Ma YJ, Sheng L, Liu HP, Liang FM, Xin GJ, Wang JH (2009) Numerical simulation for the coupling effect of local atmospheric circulations over the area of Beijing, Tianjin and Hebei Province. Sci China (Ser D Earth Sci) 52(3):382–392

Lv BL, Zhang B, Bai YQ (2016) A systematic analysis of $PM_{2.5}$ in Beijing and its sources from 2000 to 2012. Atmos Environ 124:98–108

Miao YC, Liu SH, Zheng YJ, Wang S, Chen BC (2014) Numerical study of the effects of topography and urbanization on the local atmospheric circulations over the Beijing-Tianjin-Hebei. Adv Meteorol, China. https://doi.org/10.1155/2014/397070

Miao YC, Liu SH, Zheng YJ, Wang S (2015a) Modeling the feedback between aerosol and boundary layer processes: a case study in Beijing. Environ Sci Pollut Res, China. https://doi.org/10.1007/s11356-015-5562-8

Miao YC, Liu SH, Zheng YJ, Wang S, Liu ZX, Zhang BH (2015b) Numerical study of the effects of local atmospheric circulations on a pollution event over Beijing–Tianjin–Hebei, China. J Environ Sci 30:9–20

Miao YC, Liu SH, Zheng YJ, Wang S, Liu ZX, Zhang BH (2015c) Numerical study of the effects of Planetary Boundary Layer structure on the pollutant dispersion within built-up areas. J Environ Sci 32:168–179

Miao YC, Hu XM, Liu SH, Qian TT, Xue M, Zheng YJ, Wang S (2015d) Seasonal variation of local atmospheric circulations and boundary layer structure in the Beijing-Tianjin-Hebei region and implications for air quality. J Adv Model Earth Syst 7:1–25

Miao L, Liao XN, Wang YC (2016) Diurnal variation of PM2.5 mass concentration in Beijing and influence of meteorological factors based on long term date. Environ Sci 37(8):2836–2846 **(in Chinese)**

Miao YC, Guo JP, Liu SH, Liu H, Li ZQ, Zhang WC, Zhai PM (2017) Classification of summertime synoptic patterns in Beijing and their associations with boundary layer structure affecting aerosol pollution. Atmos Chem Phys 17:3097–3110

Mosedale TJ, Stephenson DB, Collins M, Mills TC (2006) Granger causality of coupled climate processes: ocean feedback on the north Atlantic oscillation. J Clim 19(7):1182–1194

Pan X, Liu Y, Fan X (2015) Comparative assessment of satellite-retrieved surface net radiation: an examination on ceres and srb datasets in china. Remote Sens 7(4):4899–4918

Ren GY (2015) Urbanization as a major driver of urban climate change. Adv Clim Change Res 6(1):1–6

Ren GY, Chu ZY, Chen ZH, Ren YY (2007) Implications of temporal change in urban heat island intensity observed at Beijing and Wuhan stations. Geophys Res Lett 34:L05711

San Martini F, Christa A, Hasenkopf David C, Roberts (2015) Statistical analysis of PM2.5 observations from diplomoatic facilities in China. Atmos Environ 110:174–185

Smith RL, Wigley ML, Santer BD (2003) A bivariate time series approach to anthropogenic trend detection in hemispheric mean temperature. J Clim 16:1228–1240

Stedman JR (2004) The predicted number of air pollution related deaths in the UK during the August 2003 heat wave. Atmos Environ 38(8):1087–1098

Tan SC, Zhang X, Wang H, Chen B, Shi GY, Shi C (2017) Comparisons of cloud detection among four satellite sensors on severe haze days in eastern China. Atmos Ocean Sci Lett. https://doi.org/10.1080/16742834.2017.1381547

Tang YX, Zhang XL, Xu J (2016) Multi-temporal scale variations of atmospheric pollutants concentrations in rural and urban areas of Beijing. Acta Sci Circumst 36(8):2783–2793 **(in Chinese)**

Triacca U (2001) On the use of granger causality to investigate the human influence on climate. Theor Appl Climatol 69(3–4):137–138

Triacca U (2005) Is Granger causality analysis appropriate to investigate the relationship between atmospheric concentration of carbon dioxide and global surface air temperature? Theor Appl Climatol 81(3–4):133–135

Wang WL, Anderson BT, Kaufmann RK, Myneni RB (2004) The relation between the north atlantic oscillation and ssts in the north atlantic basin. J Clim 17(24):4752–4759

Wang XR, Miao SG, Dou JX, Dong F, Wang JL (2016) Observation and analysis of the air pollution impacts on radiation balance of urban and suburb in Beijing. Chinese J Geophys 59(11):3996–4006. (**in Chinese**)

Weng Q, Yang S (2004) Managing the adverse thermal effects of urban development in a densely populated Chinese city. J Environ Manag 70(2):145–156

Wu H, Wang TJ, Fang H, Ma YP, Han YQ, Huang S, Yao YA, Shi JQ (2014) Impacts of aerosol on the urban heat island intensity in Nanjing. Trans Atmos Sci 37(4):425–431 **(in Chinese)**

Xu P, Hao QJ, Ji DS, Zhang JK, Liu ZR, Hu B, Wang YS, Jiang CS (2014) Observation of Atmospheric Pollutants in the Urban Area of Beibei District, Chongqing. Environ Sci 35(3):820–829 (**in Chinese**)

Yan ZW, Li Z, Li QX, Jones P (2010) Effects of site-change and urbanisation in the Beijing temperature series 1977–2006. Int J Climatol 30(8):1226–1234

Yan HR, Huang JP, Minnis P, Wang TH, Bi JR (2011) Comparison of ceres surface radiation fluxes with surface observations over loess plateau. Remote Sens Environ 115(6):1489–1500

Yang P, Ren GY, Liu WD (2013a) Spatial and temporal characteristics of Beijing urban heat island intensity. J Appl Meteor 52(8):1803–1816

Yang YJ, Wu BW, Shi CE, Zhang JH, Li YB, Tang WA, Wen HY, Zhang HQ, Shi T (2013b) Impacts of urbanization and station-relocation on surface air temperature series in Anhui Province, China. Pure Appl Geophys 170:1969–1983

Yao Q, Cai ZY, Zhang CC, Mu HB (2010) Variety characteristics and influence factors of aerosol mass concentrations in Tianjin city. Ecol Environ Sci 9(9):2225–2231 **(in Chinese)**

Yu QW, Alexis KH, Jimmy CH, Deng XJ, Mai BR, Li F, Zou Y (2016) Exploring Granger causality of global carbon dioxide concentration and the urbanization effect for temperature trends in Hong Kong over the period 1886–2012. J Trop Meteorol 32(6):855–863

Zhang Q (2003) A study of the interaction between concentration of pollutants and the climatic and environmental factors of Lanzhou. J Lanzhou Univ 39(1):99–106 **(in Chinese)**

Zhao H, Che H, Zhang X, Ma Y, Wang Y, Wang H, Wang Y (2013) Characteristics of visibility and particulate matter (PM) in an urban area of Northeast China. Atmos Pollut Res 4(4):427–434

Zhao L, Lee X, Smith RB, Oleson K (2014) Strong contributions of local background climate to urban heat islands. Nature 511:216–219

Zhang L, Ren GY, Liu J, Zhou YQ, Ren YY, Zhang AY, Feng YW (2011) Urban effect on trends of extreme temperature indices at Beijing Meteorological Station. Chinese J Geophys 54(5):1150–1159 (**in Chinese**)

Zheng F, Zhang L, Zhu J (2006) Responses of urban atmospheric boundary layer to aerosol radiative effect over complex terrains in winter. Chin J Atmos Sci 30(1):171–179 **(in Chinese)**

Zheng YJ, Miao YC, Liu SH, He P, Wang S (2017) Analysis of meteorological variables in Dianzhong region in recent 51 years. Acta Sci Natu Univ Pekin 53(1):8–18 **(in Chinese)**

Zheng ZF, REN GY, GAO H (2018) Analysis of the phenomenon of local circulation in Beijing Area. Meteor Mon 44(3):425–433 **(in Chinese)**